Accepted manuscript version. Please cite this article as:
B. Ortega-Delgado, F. Giacalone, A. Cipollina, M. Papapetrou, G. Kosmadakis, A. Tamburini, G. Micale, *Boosting the performance of a Reverse Electrodialysis – Multi-Effect Distillation Heat Engine by novel solutions and operating conditions*, Applied Energy, 253 (2019) 113489, https://doi.org/10.1016/j.apenergy.2019.113489

Boosting the performance of a Reverse Electrodialysis – Multi-Effect Distillation Heat Engine by novel solutions and operating conditions

B. Ortega-Delgado[a], F. Giacalone[a], A. Cipollina[a,*], M. Papapetrou[a,b], G. Kosmadakis[b,c], A. Tamburini[a], G. Micale[a]

[a]Dipartimento di Ingegneria, Università degli Studi di Palermo (UNIPA),
Viale delle Scienze Ed.6, 90128, Palermo, Italy

[b]Wirtschaft und Infrastruktur GmbH & Co Planungs-KG (WIP),
Sylvensteinstr. 2, 81369, Munich, Germany

[c]Ricreation IKE, Technological Park "Lefkippos",

Patriarchou Grigoriou & Neapoleos 27, 15341, Agia Paraskevi, Greece

e-mail: andrea.cipollina@unipa.it

ABSTRACT

This work presents a performance analysis of a waste-heat-to-power Reverse Electrodialysis Heat Engine (RED-HE) with a Multi-Effect Distillation (MED) unit as the regeneration stage. The performance of the system is comparatively evaluated using two different salts, sodium chloride and potassium acetate, and investigating the impact of different working solution concentrations and temperature in the RED unit. For both salt solutions, the impact of membrane properties on the system efficiency is analysed by considering reference ionic exchange membranes and high-performing membranes. Detailed mathematical models for the RED and MED units have been used to predict the thermal efficiency of the closed-loop heat engine. Results show that, under the conditions analysed, potassium acetate provides higher efficiency than sodium chloride, requiring a smaller MED unit (lower number of effects). The maximum thermal efficiency obtained is 9.4% (43% exergy efficiency) with a RED operating temperature of 80 °C, KAc salt solution, adopting high-performing ion exchange membranes, and with 12 MED effects. This salt has been identified as more advantageous than sodium chloride from a thermodynamic point of view for the RED-HE technology and is also recommended for a cost-effective technology implementation.

Keywords

Salinity Gradient Power; KAc; Heat-to-Power; Osmotic Power; Exergy; Heat Conversion

1. Introduction

The worldwide primary energy supply has doubled during the last four decades, with fossil fuels (coal, oil, and gas) being the energy source for more than 81% of the total share [1]. Big efforts have been devoted to the development and the promotion of power production technologies based on renewable energy sources (solar, wind, geothermal, etc.), however, there are still some drawbacks that make them less economically competitive compared with conventional methods.

Traditional power generation technologies are mostly based on fossil fuels and intended for large-scale power production, covering at least the base load. There are also technologies that provide flexibility to the electricity grids, supplied with moderate heat source temperatures, such as Organic Rankine Cycles (ORC) and Kalina cycles, though they are not suitable for very low temperatures (below 100 °C). Another power generation technology from waste heat is the thermoelectric generator [2], also suited for heat source temperatures over 100-150 °C. Waste heat recovery solutions for temperatures below 100 °C for producing either upgraded heat or cooling are the electric-driven heat pumps [3] and sorption chillers [4] respectively. Besides that, a great amount of useful heat (over 300 TWh/year only in EU [5]) is rejected to the atmosphere by the industrial sector at very low temperature level, which could be further reused to produce power. In this regard, Salinity Gradient Power - Heat Engines (SGP-HEs) have been proposed as suitable emission-free technology to convert low-grade heat into electricity [6]. These engines combine a salinity gradient technology, which harvests the energy released from the controlled mixing of two solutions at different concentrations, with a regeneration unit fed by waste heat, used to restore the original concentration of the solutions after being exploited in the SGP unit.

There are two main methods to harvest the energy released from the mixing of two solutions with different salinity: (i) Pressure Retarded Osmosis (PRO) and (ii) Reverse Electrodialysis (RED). For the former, some recent publications have been centred in the performance evaluation of the PRO process. Maisonneuve et al. [7] conducted an experimental and theoretical analysis of the process efficiency, obtaining a maximum gross power density of 7.1 W/m^2. Altaee et al. [8] presented a theoretical analysis of a closed-loop PRO power generation process using a salinity gradient source, with MED as the regeneration stage, obtaining an improved performance. Also, Maisonneuve et al. [9] developed a detailed model for PRO process including non-ideal effects such as internal and external concentration polarization and

pressure losses along the membranes. The model was used to investigate the effect of operating parameters on the performance. For the RED process, also interesting works have been published recently. Tedesco et al. [10] reported experimental results of the first RED pilot plant operated with natural water sources under real conditions. Results obtained showed a power density of 1.6 W/m^2 of cell pair, while when using artificial NaCl salt solution the power density increased to 2.7 W/m^2. Related to the closed-loop configuration, Kim et al. [11] presented a model for the closed-loop RED system using thermolytic salts (ammonium bicarbonate) for waste heat recovery. The model was experimentally validated and a maximum power density of 0.84 W/m^2 was obtained. Olkis et al. [12] presented a novel closed-loop RED system with an adsorption desalinator for the restoration of the salts. Multiple salts were investigated and the performance of the system showed great potential, about 30% of exergy efficiency. Finally, Tufa et al. [13] reviewed the latest advancements in the RED technology for power generation. They investigated the developments of membranes, stack design, use of seawater/river water and concentrated brine, etc., highlighting the main technology drawbacks for the introduction in the market.

The PRO technology uses semi-permeable osmotic membranes to draw water from a low salinity stream to a pressurized high salinity stream. The resulting permeate flux is "retarded" by the application of hydraulic pressure (lower than the osmotic pressure) in the high salinity stream, gaining pressure energy, which is then converted into mechanical energy through a hydraulic turbine [14]. Conversely, reverse electrodialysis produces electricity by means of electrochemical equilibria at membranes/solutions interface, which generate an electromotive force in the membrane pile, along with a selective passage of ions through Ion Exchange Membranes (IEMs) [13]. The main advantages of the RED compared to the PRO process are: (i) electricity is directly produced without passing through pressure-mechanical energy, (ii) suitability to operate under optimised conditions with very large salinity gradients, (iii) lower sensitivity to fouling phenomena, and (iv) larger availability of IEMs and stacks for RED applications [13] in comparison with the lack of suitable osmotic membranes and modules for PRO purposes [15]. Among the key limitations of RED technology are the lower power density produced, the availability of the water resource, and reduction in membranes performances when fed by natural waters (e.g., river water and seawater). The closed-loop RED process presents several advantages with respect to the open-loop scheme. It removes the constraint related to the location (availability of the water resources), increases the power output by proper selection of salts solutions and the salinity difference between the solutions, and also overcomes

the limitations associated with possible fouling phenomena and the presence of divalent ions, which eventually decrease the power output. With this respect, a closed-loop RED heat engine has been proposed within the EU funded RED Heat-to-power project [16], where waste heat from any industrial process is used to regenerate artificial salt solutions at the outlet of the RED process.

The RED-HE concept has been analysed in the literature using two regeneration strategies: salt extraction and solvent extraction schemes. The salt extraction scheme involves the withdrawal of the solute from the dilute solution by varying the salt solubility or using thermolytic salts. In the second case, the salinity gradient of the solutions is restored by separating the solvent from the high concentrated solution by means of thermally-driving processes such as multi-effect distillation (MED) or membrane distillation (MD).

The RED-HE system has been assessed in the literature by adopting simplified models. Tamburini et al. [17] assessed different regeneration methods and the most promising salt solutions for RED-HE applications. Results obtained showed that monovalent salts based on lithium ion and potassium acetate (KAc) provide the highest values of power density, compared with sodium chloride. Also, among the regeneration methods analysed, multi-effect distillation showed the highest performance, achieving the RED-HE a maximum thermal efficiency of about 15% (assuming membranes with enhanced properties and a very low specific thermal consumption of the MED process). The analysis performed used a very simplistic approach, several ideal assumptions, neglecting problems related to IEMs and looking only at the perspective potentials of the technology. Some of the RED-HE publications are focused on the salt extraction scheme. Kim et al. [11] developed a model for a RED system using ammonium bicarbonate (NH_4HCO_3) as working fluid in closed-loop heat engine applications, obtaining a good agreement with experimental results. Kwon et al. [18] characterized the RED-HE performance using NH_4HCO_3 and fed with waste heat. The effect of the salinity gradient, type of IEMs, inlet flow rate and intermembrane distance, was analysed, predicting a maximum power density of 0.77 W/m^2 of membrane area. Bevacqua et al. [19] experimentally evaluated the performance of a RED unit fed by ammonium bicarbonate by varying operating parameters such as solutions velocity and concentration. Results obtained showed a maximum power density of 2.4 W/m^2 of cell pair for the lowest inlet velocity (0.5 cm/s) and feed inlet concentrations of 0.04 – 2 M. Bevacqua et al. [20] presented a process model to analyse a RED-HE using NH_4HCO_3 as working fluid, with a stripping column for the salinity regeneration of the solutions. A maximum thermal efficiency of 1.2% was reported using standard IEMs, and

of 2.2% (power density of 9 W/m^2) using enhanced membranes, under the best-operating conditions found. Recently, Giacalone et al. [21] presented an experimentally validated model of a thermolytic RED-HE. A maximum exergy efficiency of 8.5% was achieved with high-performing IEMs and multi-column regeneration units. However, the low solubility limit of NH_4HCO_3 (lower than 3 M) is a big disadvantage of this salt solution, limiting the maximum driving force achievable.

Other works have been devoted to the analysis of solvent extraction regeneration scheme based on membrane distillation. Long et al. [22] analysed the impact of different heat source temperatures, permeate/feed solution flow rate ratio and inlet concentrations on the performance of the RED-HE with NaCl, showing that higher inlet concentration provides higher thermal efficiency, reaching a maximum of 1.15% with operating temperatures of 20 °C and 60 °C and feed concentration of 5 mol/kg. Similarly, Micari et al. [23] investigated the performance of a RED-MD HE fed by NaCl-water solution, starting from currently available RED and MD units and following with a perspective analysis with improved units performance. Results indicate a thermal efficiency of 0.4% using standard units' properties, and 2.8% (16.5% exergetic) using enhanced membranes and process schemes (hot and cold temperatures of 80 – 20 °C, and 5 – 0.01 M for the concentrate and dilute solutions, respectively). However, when comparing MD and MED processes as regeneration stage, the MED process is expected to provide better overall performance due to its lower specific thermal consumption (40 – 65 kWh/m^3 of distillate [24]) compared to MD (>100 kWh/m^3 [25]).

The RED-HE with MED was investigated by Hu et al. [26], who carried out a theoretical analysis of the system performance. Results related to a base case with inlet solutions concentrations of 5 – 0.05 mol/kg (concentrate-dilute) showed that increasing the initial salinity of the MED inlet solution to 3.75 mol/kg and the number of MED effects up to 10, led to an overall thermal efficiency of about 1%. Palenzuela et al. [27] also analysed the performance of a RED-HE with salt regeneration by means of a MED process. Sensitivity analyses were carried out to investigate the influence of the operating conditions on the overall performance and obtained a maximum thermal efficiency of 1.4% when using current standard reference membranes, and 6.6% with membranes with enhanced properties (high-performing membranes), showing the high potential of the heat to power conversion using this regeneration scheme. All the above efficiency values are comparable to other heat-to-power technologies, such as the ORC, which reaches 4.5% for a heat source at 100 °C [28], while the thermoelectric generators show a much lower efficiency of about 1-2% for similar temperatures [29].

As mentioned previously, one of the advantages of the closed-loop RED-HE is the possibility of selecting a suitable salt solution with specific properties able to improve the performance of the system. So far, all the published RED-HE studies with solvent extraction scheme have been carried out with sodium chloride aqueous solution as the working fluid. However, there are better performing salts for RED-HE applications. In this regard, Tamburini et al. [17] suggested lithium-based salts and potassium acetate as the most performing salts, increasing notably the power production in the RED unit. Giacalone et al. [30] analysed the properties of non-conventional salt solutions on the operation and performance of closed-loop RED with single stage and multistage evaporative regeneration. Results obtained showed that KAc provided better performance than NaCl due to its higher solubility and higher value of the activity coefficients. Also, previous works have anticipated that increasing the feed solutions temperature to the RED improves the power density of the process. Benneker et al. [31] investigated the effect of the temperature and temperature gradients on the RED process using commercial membranes. Results obtained showed an increase in the power density of about 25%. Długołecki et al. [32] assessed also the effect of the solution temperature on the RED performance, obtaining a significant increase of the stack power density when passing from 20 to 40 °C. Daniilidis et al. [33] experimentally investigated the RED performance as a function of the feed water concentration and temperature. Results showed that increasing the temperature from 25 to 60 °C almost double the value of the power density, following a linear trend. The maximum value of the power density obtained was of 6.7 W/m^2 at 60 °C. However, the effect of the working solutions temperature increase in the overall efficiency of the RED-HE has not been investigated so far, specifically considering the implications on the energy consumption of the regeneration stage.

This work analyses for the first time in the literature with a robust approach the influence of the working solution temperature in a RED-HE system using non-conventional salt solutions. In particular, the performance of the system is predicted and compared for two different salts, sodium chloride and potassium acetate, at three operating temperatures, 25, 50, and 80 °C in the RED unit, using both IEMs with standard reference properties and high-performing properties. A detailed and comprehensive mathematical model for the integrated RED-MED system has been used to carry out the comparative thermodynamic assessment between both salts. The efficiency evaluation along with the design of the single units of the integrated RED-HE represents the first step to assess the economic feasibility of the technology by estimating the levelised cost of electricity.

2. Description and modelling of the system

The RED and MED processes are described in the following subsections, together with the integrated system and the thermophysical properties of the solutions and IEMs.

2.1. Reverse Electrodialysis unit

In a RED process (see Fig. 1) electricity is produced due to the difference of chemical potential of a High Concentration solution (HC, concentrate) and a Low Concentration solution (LC, dilute). An electromotive force is induced at the solution-membrane interface and an electrical current generated by the controlled mixing of both solutions, i.e. when ions selectively pass between the HC and LC channels. Cationic and anionic IEMs are disposed in alternative positions forming a stack of membranes and channels. At both sides of the stack, a cathode and an anode are disposed within a rinse solution, which is used to generate a redox reaction and convert the current of ions in a current of electrons flowing in an electrical circuit closed with an external load.

The mathematical model of the RED process used in this work has been adapted from [34], including pressure losses and polarization effects. The model has been validated against experimental data in [34], and it has implemented in Engineering Equation Solver (EES) [35]. The model has a hierarchical structure: in the lower level, concerning the cell pair (formed by a concentrated channel, a dilute channel, a CEM and an AEM), the mass balance and transport equations for water and salt are applied, together with the equations of the equivalent electric circuit. The higher-level model includes all the cell pairs forming the stack. For the sake of brevity, only the fundamental model equations are shown here, while more information and details about the model can be found in [34].

The RED model is numerically solved on a discretized domain over the length of the channels with N_k elements, in which the mass, transport and electrical equations are applied. The electromotive force of the cell pair $E_{cell,k}$ (V) for each k-element is determined by:

$$E_{cell,k}(T,C) \cong 2\alpha_{av,k}(T,C)\frac{R_g T}{F}\ln\left(\theta^{HC}_{IEM,k}(T,C)\cdot\theta^{LC}_{IEM,k}(T,C)\frac{m_{HC,k}\cdot\gamma_{HC}(T,C)}{m_{LC,k}\cdot\gamma_{LC}(T,C)}\right) \quad (1)$$

where α (-) is the permselectivity of the membranes, R_g (8.314 J/(mol·K)) the universal gas constant, T (K) the average solutions temperature, F (96,485.3 s·A/mol) the Faraday constant, θ (-) is the polarization coefficient (determined using Eqs. S3 and S4 of the Supplementary Information), m (mol/kg) the molality of the solution, and γ (-) the activity coefficient (calculated with the Pitzer's ion-interaction model, described in Supplementary Information). The electrical resistance of the cell pair for each k-element is defined by:

$$R_{cell,k}(C,T) = \left[R^{sol}_{HC,k}(C,T) + R^{sol}_{LC,k}(C,T) + R_{CEM,k}(C,T) + R_{AEM,k}(C,T)\right]\cdot\frac{1}{b\Delta x} \quad (2)$$

where R^{sol}_{HC} and R^{sol}_{LC} ($\Omega\cdot m^2$) are the areal resistance of the HC and LC solutions, R_{CEM} and R_{AEM} ($\Omega\cdot m^2$) the areal resistance of the cationic and anionic membranes, b (m) is the width of the membrane, and Δx (m) the length of each discretization step.

The electric current i (A) in each branch of the equivalent electric circuit is determined by Eq. (3):

$$i_k(T,C) = \frac{N_{cp}\cdot E_{cell,k}(T,C) - (R_{blank}I/A_{cp} + E_{stack})}{N_{cp}\cdot R_{cell,k}(T,C)} \quad (3)$$

where N_{cp} (-) is the number of cell pairs, R_{blank} (Ω) is the electrical resistance of the electrodic compartments, I (A) is the total current flowing in the external circuit, A_{cp} (m^2) is the area of the cell pair, and E_{stack} (V) is the voltage drop in the external load circuit, calculated with Eq. (4):

$$E_{stack} = R_L\cdot I \quad (4)$$

where R_L (Ω) is the electrical resistance of the external load.

The gross power (W) produced is obtained by Eq. (5):

$$P_{gross} = E_{stack}\cdot I = I^2\cdot R_L \quad (5)$$

where I (A) is the electrical current. The net power P_{net} (W) is calculated by subtracting the pumping power consumption to the gross power:

$$P_{net} = P_{gross} - P_{pump,RED} \tag{6}$$

with:

$$P_{pump,RED} = \frac{\Delta p_{HC} Q_{HC}}{\eta_{p,HC}} + \frac{\Delta p_{LC} Q_{LC}}{\eta_{p,LC}} \tag{7}$$

where Δp (Pa) is the pressure loss across the stack (inlet-outlet, see Supplementary Information), Q (m^3/s) the volumetric flow rate, and η_p (-) the pump efficiency, for each of the two streams (HC and LC). The power density (W/m_{cp}^2) of the RED unit can be calculated according to Eq. (8):

$$P_d = \frac{P_{net}}{A_{cp} \cdot N_{cp}} \tag{8}$$

Transport equations for determining the water and salt fluxes and differential mass balance equations needed to close the model are not reported here for the sake of brevity but can be found in [34].

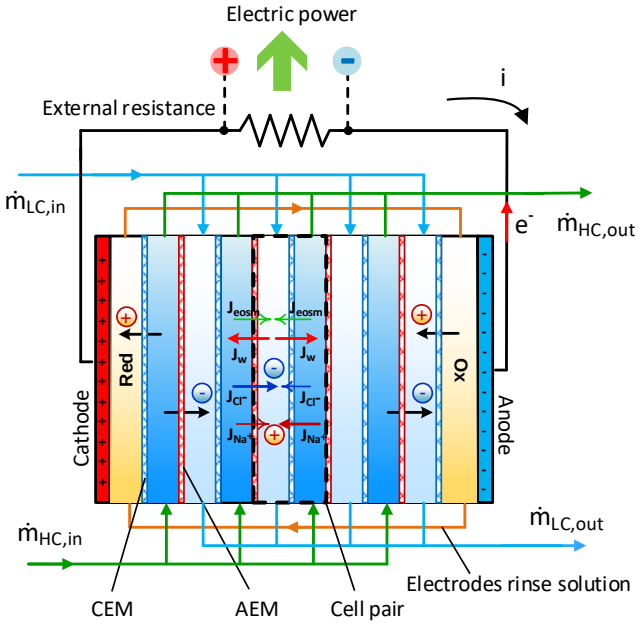

Fig. 1. Scheme of the reverse electrodialysis process, showing the inlet and outlet solutions flow rate of the low concentration (LC) solution and the high concentration (HC) solution, and the salt and water fluxes within a cell pair.

2.2. Multi-effect distillation unit

The MED unit is used in the RED-HE to restore the initial concentrations of the solutions, once they have passed through the RED unit. The MED process is widely used in the chemical and food industry since the beginning of the 20th century, but it found also an important application in the seawater desalination field [36]. Due to the higher thermal performance in comparison with other processes such as multistage flash, it has become more and more used in recent years and has been selected for the regeneration of the salinity gradient of the solutions in the present RED-HE application.

The MED process, depicted in Fig. 2, basically separates a solvent (water) from a concentrate (brine) by a sequence of evaporation and condensation stages, which take place inside the MED effects. In this work the forward-feed (FF) vertical stack scheme is chosen, where the vapour and the brine follow the same descendent direction within the unit. The main elements constituting the MED process are evaporators, preheaters, flash boxes, and end condenser. External heat (usually from the latent heat of condensing steam) is introduced inside the tube bundle of the first evaporator, located at the top of the unit. The feed water is sprayed over the tube bundle and partially evaporates, while the rest of the feed water, more concentrated, falls to the bottom of the effect, and is directed to the next effect as feed. The vapour produced is used in part to preheat the feed water in the preheater (PH), and the rest as motive steam in the next evaporation-condensation process of the following effect. The distillate produced in the evaporator and preheater is collected in a flash box (FB). Apart from the vapour produced by the evaporation of feed water, flash vapour is generated in the flash boxes (from distillate) and at the entrance of the effects (from the second to the last), due to the sudden reduction in the ambient pressure passing from one effect to the other. The vapour produced in the last effect is condensed in the final condenser, using a cooling stream. Two plate heat exchangers are used to cool down the concentrate and distillate streams to 25 °C before leaving the unit, using cooling water.

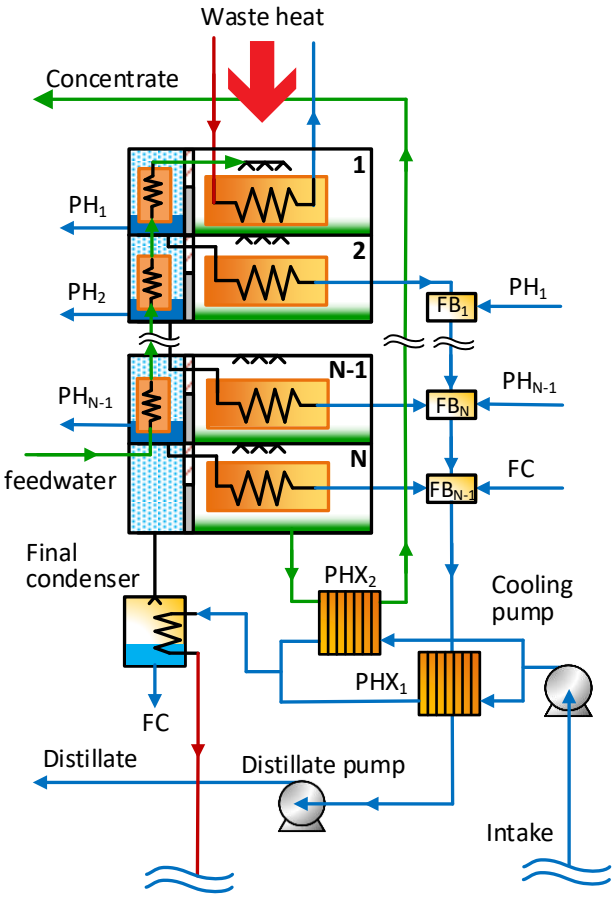

Fig. 2. Scheme of the multi-effect distillation unit, showing the main elements: effects, preheaters (PH), evaporators, flashing boxes (FB), final condenser, plate heat exchangers (PHX) and pumps.

The model of the FF-MED, implemented in Engineering Equation Solver (EES), has been adapted from [37] to be suitable for the simulation of this process, in a wide range of operating conditions and with a high number of effects. The model has been validated in [37]. The number of effects is selected taking into account the total temperature difference between the heat source (at 100 °C) and the cooling water (15 °C), together with a minimum temperature driving force in each effect (mean effective temperature difference). In this regard, is important to note that the boiling point elevation of the solution is a loss for the MED process. The higher the BPE, the lower the total available temperature difference in the MED unit. As sodium chloride has on average lower BPE than potassium acetate, a higher number of effects can be considered, and accordingly higher thermal efficiency (see Section 4).

The performance of the MED is defined by the specific thermal energy consumption sE ($kWh/m^3_{distillate}$):

$$sE = \frac{\dot{m}_s \lambda_s}{\dot{m}_D / \rho_D} \cdot \frac{1}{3600} \tag{9}$$

where $\dot{m}_s$ (kg/s) is the mass flow rate of the steam entering the first effect, λ_s (kJ/kg) is the enthalpy of vaporization of water, $\dot{m}_D$ (kg/s) is the mass flow rate of the distillate produced, and ρ_D (kg/m^3) is the density of the distillate. Another relevant parameter of the MED unit is the specific heat transfer area sA, (m^2/(kg/s)), i.e. the heat exchanger area required per mass flow rate unit of distillate:

$$sA = \frac{\sum_{i=1}^{N} A_i + \sum_{i=1}^{N-1} A_{preh,i} + A_c}{\dot{m}_D} \tag{10}$$

where A_i (m^2) is the surface area of the evaporator i, $A_{preh,i}$ (m^2) is the surface area of the preheater i, and A_c (m^2) is the surface area of the final condenser.

The pumping power needed for the MED process, $P_{pump,MED}$ (W), calculated with Eq. (11), accounts for the hydraulic pumping head required to pump water up to the top of the unit $\Delta p_{MED,H}$ (Pa), the pumping to the atmospheric pressure of the outlet concentrate and dilute streams, $\Delta p_{MED,HC,out}$ (Pa) and $\Delta p_{MED,D,out}$ (Pa), respectively, and the pressure drops in the end condenser $\Delta p_{MED,cooling}$ (Pa) (see Supplementary Information file for more details).

$$\begin{aligned} P_{pump,MED} = {} & \frac{\Delta p_{MED,H} \cdot Q_{MED,HC,in}}{\eta_{p,f}} + \frac{\Delta p_{MED,HC,out} \cdot Q_{MED,HC,out}}{\eta_{p,HC}} \\ & + \frac{\Delta p_{MED,D,out} \cdot Q_{MED,dist,out}}{\eta_{p,D}} + \frac{\Delta p_{MED,cooling} \cdot Q_{cw}}{\eta_{p,c}} \end{aligned} \tag{11}$$

where $Q_{MED,HC,in}$ (m^3/s) and $Q_{MED,HC,out}$ (m^3/s) are the volumetric flow rates of the HC solution at the inlet and outlet of the MED, respectively, $Q_{MED,D,out}$ (m^3/s) is the volumetric flow rate of the distillate stream, Q_{cw} (m^3/s) is the volumetric flow rate of the cooling water, and $\eta_{p,f}$ (-), $\eta_{p,HC}$ (-), $\eta_{p,D}$ (-), and $\eta_{p,c}$ (-) are the isentropic efficiencies of the pumps.

2.3. Integrated system

Two different schemes are considered for the RED-MED HE: one operating the RED unit at room temperature (25 °C), and the second one, aimed for higher RED operation temperature (reheat option). The first arrangement, depicted in Fig. 3, consists of a RED and MED units

integrated with two mixers (Mixer 1 and Mixer 2). In the RED unit, a high concentration solution ($\dot{m}_{HC}$) and a low concentration solution ($\dot{m}_{HC}$) enter the stack. The salinity gradient established between both solutions generates a certain amount of power thanks to the controlled mixing process. At the outlet of the RED unit, the HC solution has lost salinity, while the dilute solution has gained it. The amount of salt lost in the concentrate loop is restored in Mixer 1 by adding to it part of the dilute solution ($\dot{m}_{bypass}$). The resulting solution ($\dot{m}_{MED,in}$) enters the MED unit where, by thermal separation of the solvent (evaporation), the original concentration of the HC solution is restored. The distillate produced in the MED unit ($\dot{m}_D$) is then mixed with the dilute solution ($\dot{m}_{LC,M2,in}$) in Mixer 2 to recover its original concentration and mass flow rate. In this scheme, two plate heat exchangers (PHX_1 and PHX_2) are used in the MED unit to cool down the produced concentrate and distillate solutions to room temperature.

In the second arrangement (see Fig. 4), the scheme is modified by introducing two reheaters (RH_1 and RH_2) that warm up the concentrate and dilute solutions with part of the external waste heat. Two tubular HXs in counterflow arrangement, namely HX_1 and HX_2, are used to preheat the concentrate and distillate streams at the outlet of the MED by exchanging sensible heat from the HC solution to be regenerated, which has to be cooled down before entering the MED unit. Moreover, another mixer (Mixer 3) is added at the inlet of the MED unit where the concentrate solutions at the outlet of the HXs are mixed.

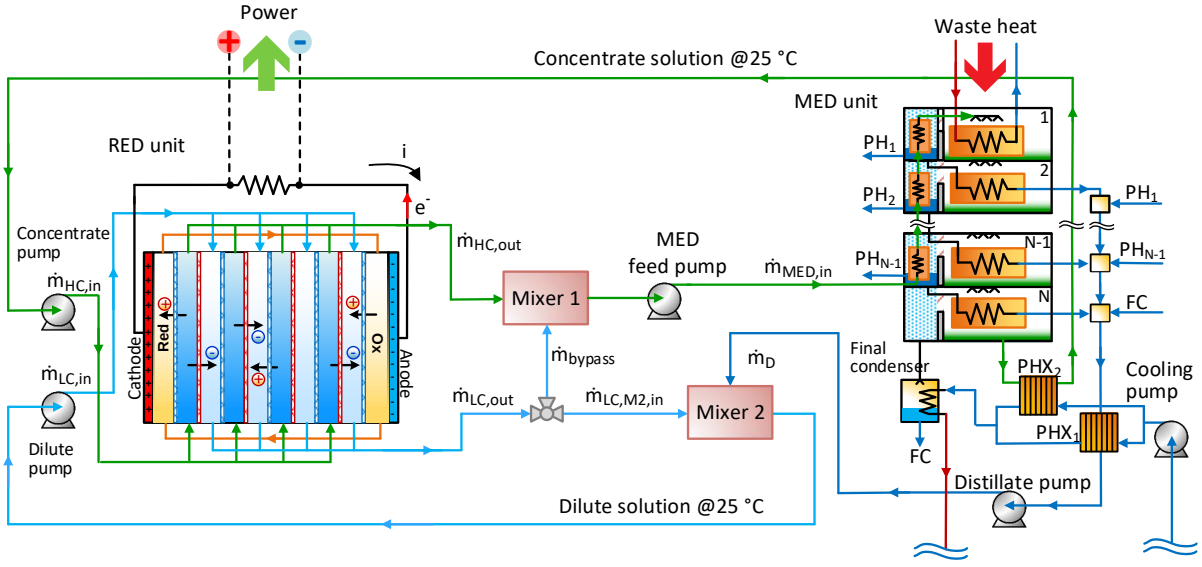

Fig. 3. Schematic of the RED-MED HE system for a working fluid at room temperature (25 °C). Note that the PHXs in the MED are used to cool down the concentrate and distillate solutions to 25 °C.

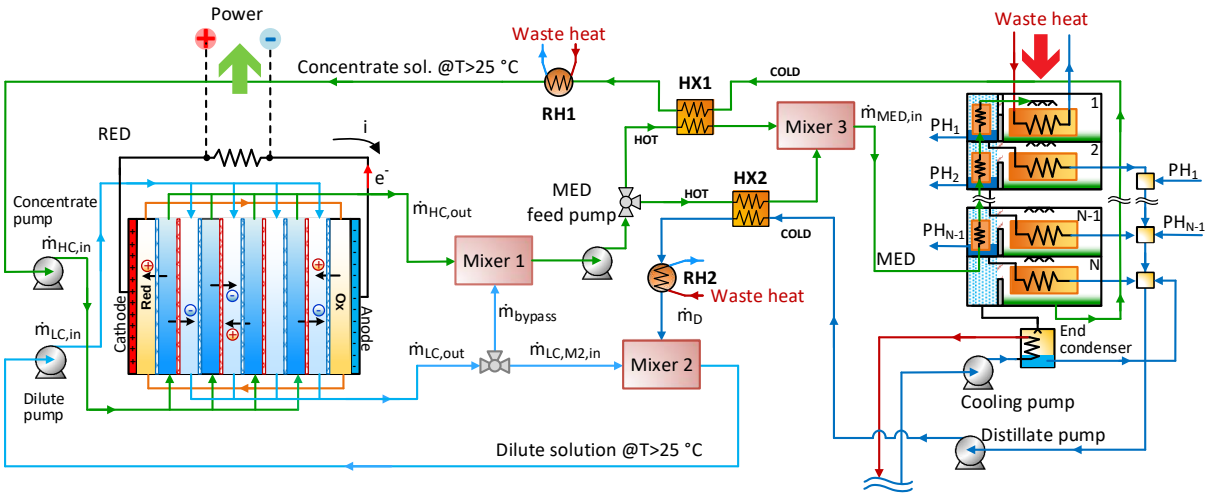

Fig. 4. Schematic of the RED-MED HE system for high working fluid temperature (>25°C). Note that in this case two reheaters (RH) are used to heat up the concentrate and distillate streams to the temperature required in the RED pile. Also, the waste heat requirements are reduced using thermal integration (heat exchangers HX1 and HX2).

The governing equations of the integrated system operating at room temperature are thoroughly described in [27]. In the second scheme, the equation for the mass balance in Mixer 3 is included. This mixer is assumed to operate in isothermal conditions. Moreover, for the design of the HXs, the overall heat transfer coefficient is assumed as 1000 (W/m^{2}K) [38], while the temperature difference between the inlet hot stream and the warmed-up outlet cold stream is fixed to 5 °C. The heat exchangers have been modelled with the NTU-effectiveness method [39].

The thermal efficiency of the integrated system is defined as the ratio of the net power produced in the RED unit, P_{net} (gross power minus the RED and MED pumping power), and the thermal power input in the regeneration stage, $P_{Q,wh}$:

$$\eta_{th} = \frac{P_{net}}{P_{Q,wh}} = \frac{P_{gross} - P_{pump,RED} - P_{pump,MED}}{P_{Q,wh}} \quad (12)$$

The exergy efficiency of the global system η_X (-) can be defined as the thermal efficiency divided by the ideal efficiency of a Carnot heat engine working between the waste heat temperature T_{wh} (in K) and the cooling water temperature T_{intake} (in K):

$$\eta_X = \frac{P_{net}}{P_{Q,wh}\left(1 - \frac{T_{wh}}{T_{intake}}\right)} = \frac{\eta_{th}}{1 - \frac{T_{wh}}{T_{intake}}} \quad (13)$$

2.4. Thermophysical properties of solutions and IEMs

The thermo-physical properties of solutions play a fundamental role in determining the performance of the RED-HE. Salt solutions with high solubility allow for higher concentration gradients and hence higher voltage generated in the pile (see Eq. (1)). Similarly, concentrate solutions with high activity coefficients lead to a higher electromotive force generation in the RED unit. The integrated RED-MED HE model needs the properties of the working solutions to be defined in order to quantify the power output. In particular, the correlations used to estimate the thermo-physical properties (density, boiling point elevation, specific heat, enthalpy, etc.) of the adopted sodium chloride and potassium acetate solutions are reported in the Supplementary Information file. The hydrations numbers considered for determining the electro-osmotic flux through the IEMs using NaCl and KAc salts are 7 [40] and 7.9 [41], respectively. The osmotic and activity coefficients have been estimated using the Pitzer's ion-interaction model [42], reported in the Supplementary Information file.

FujiFilm Manufacturing Europe B.V. has provided data for the properties of standard reference Type 10 membranes using NaCl and KAc aqueous solutions. The properties are electrical resistance, permselectivity, salt permeability, and water permeability (see Fig. 5). Trends of permselectivity and electrical resistance have been correlated as a function of temperature and concentration, while for permeabilities only the dependence with the temperature is considered. Trends have been extrapolated up to 80 °C in cases where no information was available. For the salt and water permeability with NaCl salt, the same temperature variation trend as KAc has been assumed, due to the lack of experimental data at temperatures higher than 25 °C (see Fig. 5e-h).

Figs. 5a-b show experimental data and trends of the electrical resistance of the membrane as a function of the temperature for different inlet molar concentrations of the concentrate solution. It can be seen how a higher temperature of the solution leads to a lower resistance both for NaCl and KAc salts, although at low concentrations the resistance of KAc is clearly higher than that of the NaCl. However, for higher temperatures, the resistance with KAc is lower than in the case of NaCl. The variation of the permselectivity values with NaCl and KAc salts are depicted

in Figs. 5c-d, respectively. The increasing temperature reduces the permselectivity, which is in general higher for KAc than for NaCl. The salt permeability is presented in Fig. 5e-f. In this case, the increase of temperature increases the salt permeability and therefore the salinity gradient is reduced within the pile. Comparing both salts, the salt permeability is significantly higher (about four times) for the case of NaCl. Finally, the water permeability as a function of the temperature of the solution for NaCl and KAc are reported in Figs. 5g-h. The trend is also increasing with temperature, and the values for both salts are similar.

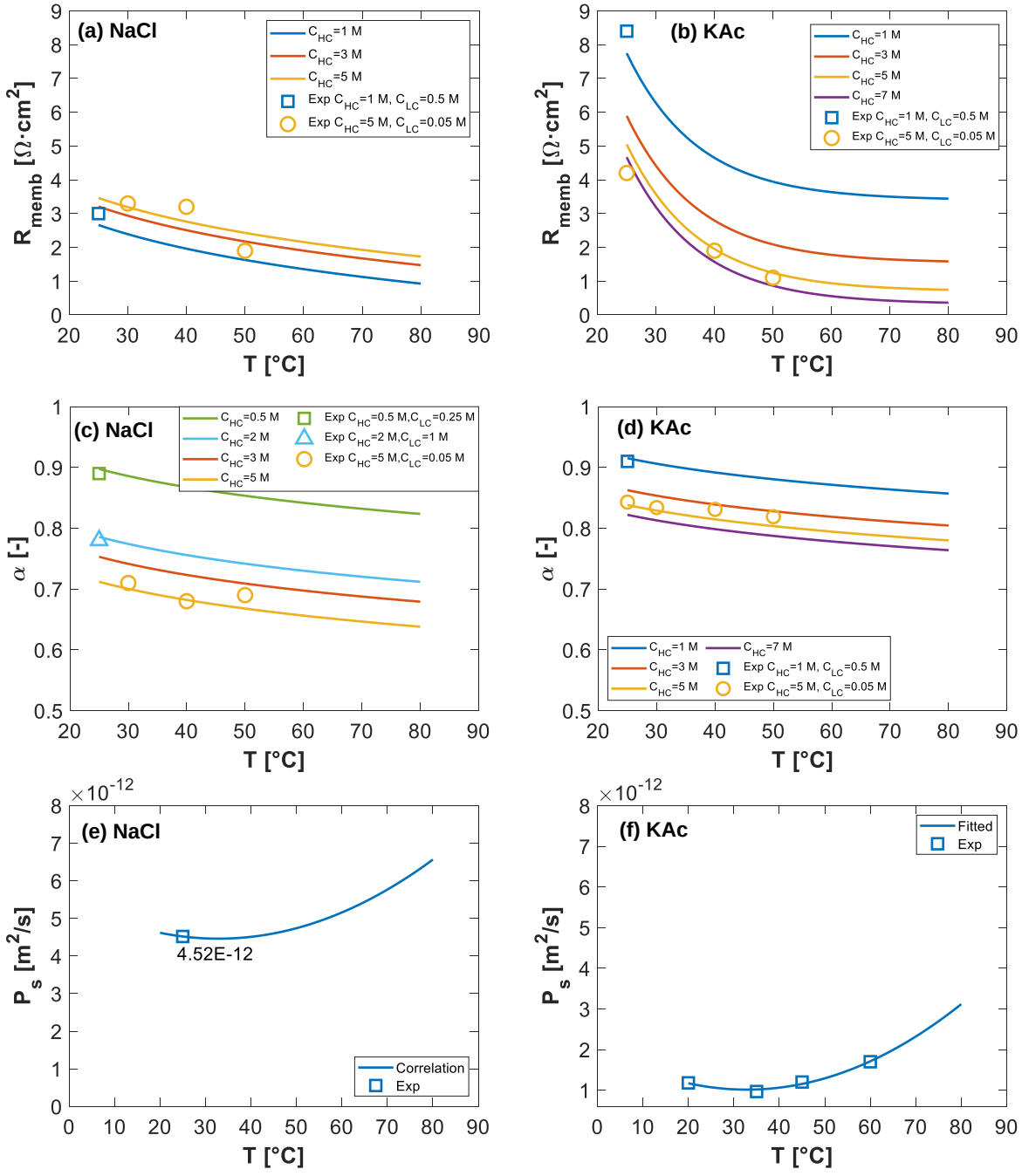

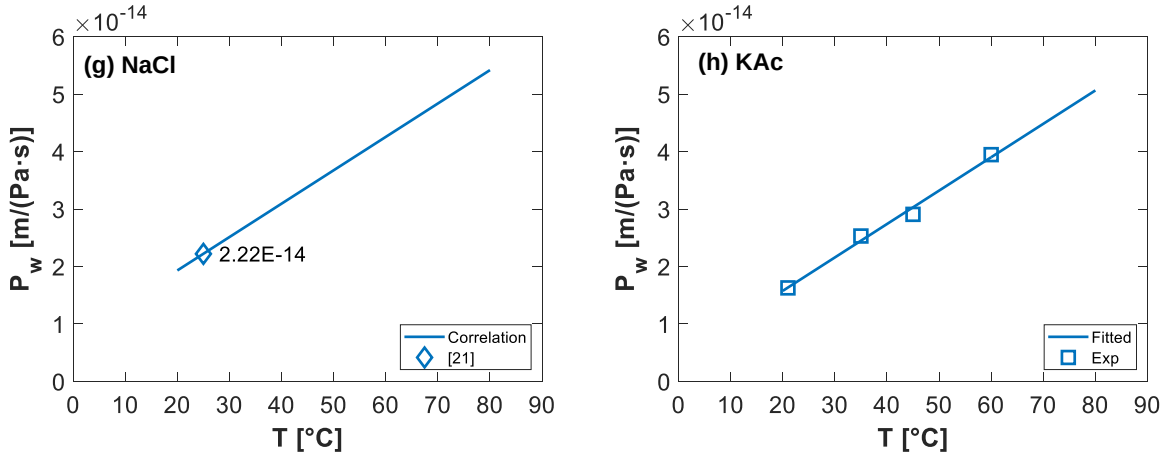

Fig. 5. Membrane properties variation with temperature, for NaCl and KAc salts: (a-b) Electrical resistance, (c-d) permselectivity, (e-f) salt permeability, and (g-h) water permeability. Experimental data (symbols) and correlation trends (lines).

In order to perform a perspective analysis of the technology, also membranes with enhanced properties, named high-performing membranes, were considered. The electrical resistance is decreased to one eight of the reference IEM value in the specified conditions, the permselectivity is kept equal to 98% in all the concentration and temperature range, while the salt and water permeabilities are decreased to one-fourth of the reference IEM value in the conditions examined. Sample values of the properties of these membranes for 0.5 M and 25 °C are reported in Table 1 and are in line with several high-performing IEMs available in the market [23].

Table 1. Sample values of the IEMs properties measured at 0.5 M and 25 °C, for reference and high-performing membranes. Note that the properties of the IEMs are changing with the concentration and/or temperature.

	Reference IEMs		**High-performing IEMs**	
	NaCl	**KAc**	**NaCl**	**KAc**
Electrical resistance, R_{av} (Ω·cm^2)	2.3	8.5	0.3	1.1
Permselectivity, α_{av} (%)	90	95	98	98
Salt permeability, P_s (m^2/s) ×10^{12}	4.52	1.07	1.13	0.27
Water permeability, P_w (m/(Pa·s)) ×10^{14}	2.22	1.87	0.56	0.47

* Resistance=1/8 of reference value; Permselectivity=98%; Salt and water permeabilities=1/4 of reference value.

3. Methods

Firstly, the performance of the RED-MED system is analysed using sodium chloride and potassium acetate solutions for a fixed number of MED effects, under a reference scenario defined in Table 2 and Table 3. The HC inlet concentration and the temperature of the solutions in the RED unit are varied while maintaining the rest of the variables constant. Specifically, the inlet HC solution concentration is varied in the range 3 – 5 M for NaCl and 3 – 7 M for KAc, while the LC solution concentration is kept equal to 0.01 M. Three different operating temperatures in the RED unit are investigated: 25 °C (room temperature), 50 °C and 80 °C (high temperature). This analysis is carried out using standard reference IEMs properties (Type 10) provided by FujiFilm, with woven spacers thick of 1.5×10^{-4} m for both channels, a relative spacer volume of 0.175 and a shadow factor of 1.563. Pumps efficiency is assumed to be of 80%.

Table 2. Input variables of the RED unit model in the reference scenario.

Concept	**Value**
Cell pair	
Flow pattern	Counter-current
Number of cell pairs, (-)	1000
Width, b (m)	0.25
Length, L (m)	1
Operation temperature, T (°C)	Variable (25, 50, 80)
Solutions	
Concentrate inlet concentration, C_{HC} (mol/L)	Variable (3 – 5)
Dilute inlet concentration, C_{LC} (mol/L)	0.01
Inlet concentrate velocity, v_{HC} (cm/s)	0.25
Inlet dilute velocity, v_{LC} (cm/s)	1

Table 3. Input variables for the MED unit model in the reference scenario.

Concept	**Value**
Number of effects, (-)	Variable[a]
Heating steam temperature, (°C)	100
Final condenser ΔT, (°C)	5
Terminal temp. difference preheater 1, (°C)	3
Intake cooling water temperature, (°C)	15

Falling-film evaporators	
Tube length, (m)	1
Tube outer diameter, (m)	0.011
Tube inner diameter, (m)	0.01
Distance between tubes, (m)	0.0095
Steam velocity inside tubes[b], (m/s)	50
Preheaters (S&T)	
Tube length, (m)	1
Tube outer diameter, (m)	0.011
Tube inner diameter, (m)	0.01
Feedwater velocity[b], (m/s)	0.5
Number of tube passes, (-)	1
End condenser (S&T)	
Tube length, (m)	2
Tube outer diameter, (m)	0.022
Tube inner diameter, (m)	0.02
Feedwater velocity[b], (m/s)	1
Number of tube passes, (-)	2

[a] Equal to 12 for the reference case.
[b] [43]

The influence of the number of MED effects on the overall thermal efficiency and specific heat transfer area is investigated, for both NaCl and KAc solutions and using standard reference and high-performing membranes, whose properties are depicted in Table 1. The inlet solutions concentration and velocity to the RED unit used in the simulations are reported in Table 4. These values were obtained by a preliminary assessment, which is not shown here for the sake of brevity, where a parametric analysis of the performance was carried out in a discretized range of concentration and velocity of the solutions, identifying the optimal combination leading to maximize the overall thermal efficiency.

Table 4. Inlet solutions concentration and velocity used for the analysis of the RED-MED performance at room (RT) and high temperature (HT), for both standard reference IEMs and high-performing IEMs.

Concept	**NaCl**		**KAc**	
	RT	HT	RT	HT
HC solution concentration, (mol/L)	3.8 (5)*	5	6	7
LC solution concentration, (mol/L)	0.01	0.01	0.01	0.01

HC solution velocity, (cm/s)	0.25 (0.4)*	0.25 (0.6)*	0.2	0.5
LC solution velocity, (cm/s)	0.8	1	0.7	1.5

*Values between brackets refer to the high-performing IEMs case only.

4. Results and discussion

This section presents the results on the comparison of the RED-MED HE performance using KAc and NaCl solutions at variable RED operating temperature. A reference case with 12 effects in the MED unit is presented first for comparison purposes, while the influence of the number of MED effects on the overall performance is later analysed. In this latter case, the use of high-performing membranes has been also considered, in order to give a perspective view of the technology potentials.

4.1. Performance comparison using KAc and NaCl salt solutions

Thermodynamic parameters and membrane properties were first analysed. Figs. 6a-c show a higher activity coefficients ratio (γ_{HC}/γ_{LC}) for KAc salt solution than that of NaCl solution in all the HC solution concentration range and for the three different operating temperatures evaluated (25, 50, and 80 °C). The increase of this parameter results in an increase of the electromotive force generated in each cell pair and therefore in the power produced in the RED unit (see Eq. (1)). However, for KAc it becomes smaller with the increase of temperature, while it is maintained approximately constant for NaCl. The membrane resistance is higher for KAc, particularly at room temperature and low concentration, but in all cases the temperature increase results in a significant reduction (see Figs. 6d-f), as mentioned previously. When passing from 25 °C to 50 °C, the reduction is higher for KAc than for NaCl, while going up to 80 °C still reduces the resistance with NaCl, while only produces a small decrease for KAc. Despite this, the increase of temperature also produces an increase of co-ions and water permeation through the ionic exchange membranes (Figs. 5e-h in the previous section), resulting in a moderate reduction of the permselectivity (Figs. 6g-i).

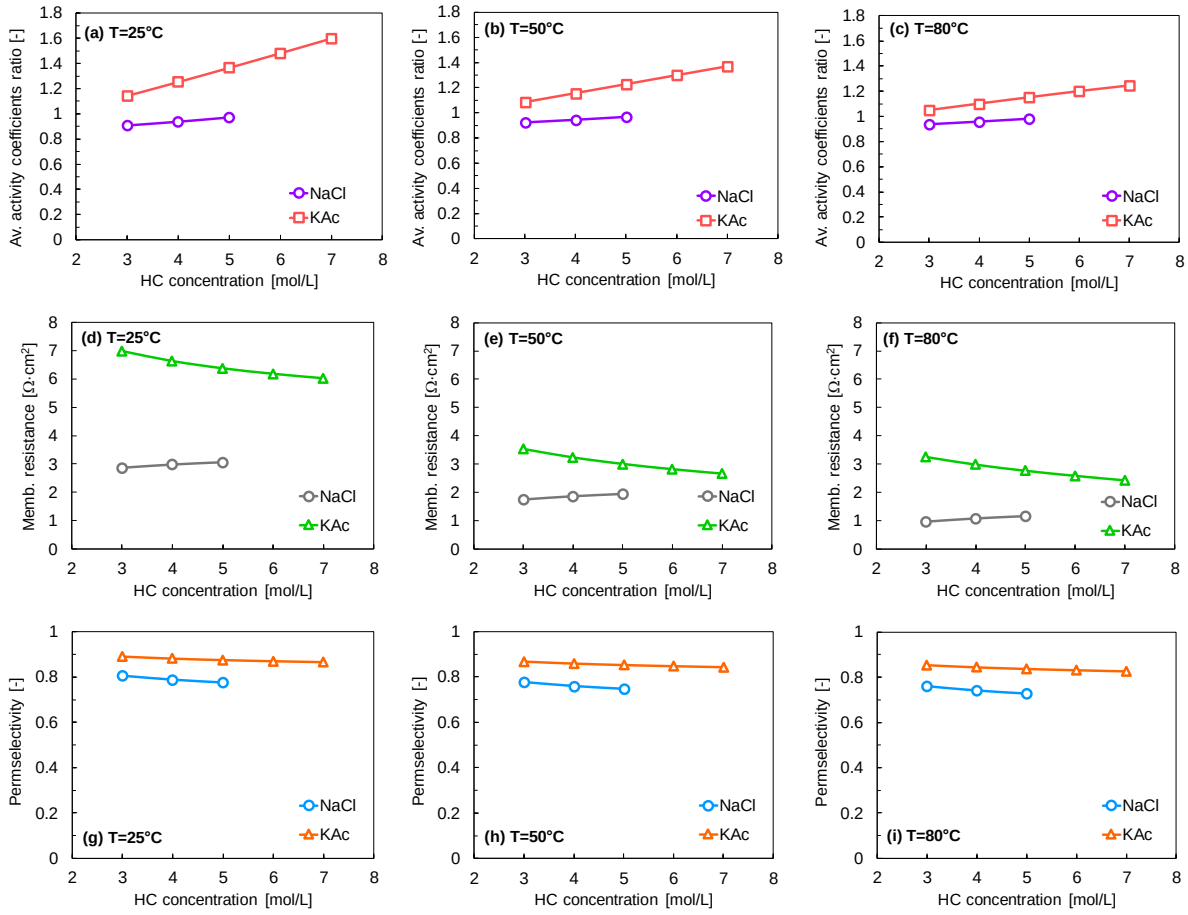

Fig. 6. Solutions and membranes properties as a function of the HC inlet concentration and operating temperature (25, 50 and 80 °C), with 12 MED effects, C_{LC}=0.01 mol/L, v_{HC}=0.25 cm/s, v_{LC}=1 cm/s, using standard reference membranes. (a)-(c) mean activity coeff. ratio, (d)-(f) membrane resistance, (g)-(i) permselectivity.

The effect of the temperature and concentration variation on the membrane and solution properties leads to the power density variation depicted in Figs. 7a-c for the RED unit. The increase of power density from 25 °C to 50 °C is more pronounced for KAc due to the higher reduction of the electrical resistance than for NaCl (60-70% in the former and around 30% in the latter, as shown in Fig. 5a-b), while the salt permeability remains approximately constant (Fig. 5e-f) and the water permeability increases linearly and in a similar way for both salts (Fig. 5g-h). However, a further increase of temperature from 50 °C to 80 °C has a different impact on the two salts: while for NaCl a marginal increase of the power density is observed, power density is reduced in the case of KAc. This can be attributed to the fact that the temperature increase from 50 to 80 °C does not lead to a significant decrease of the resistance for KAc, while the salt and water fluxes are twice or three times larger.

Finally, the thermal and exergy efficiency follows the trend of power density, being higher for KAc in all the concentration and temperature ranges (see Figs. 7d-f). In particular, the efficiency for KAc is more than twice than for NaCl at 50°C: 1.4% vs 0.6% (thermal) and 6% vs 2.6% (exergetic). The higher efficiencies obtained using KAc salt can be attributed to its higher solubility, which extends the concentration range available for the HC solution, higher activity coefficients ratio (Figs. 6a-c), and higher IEMs permselectivity (Figs. 6g-i).

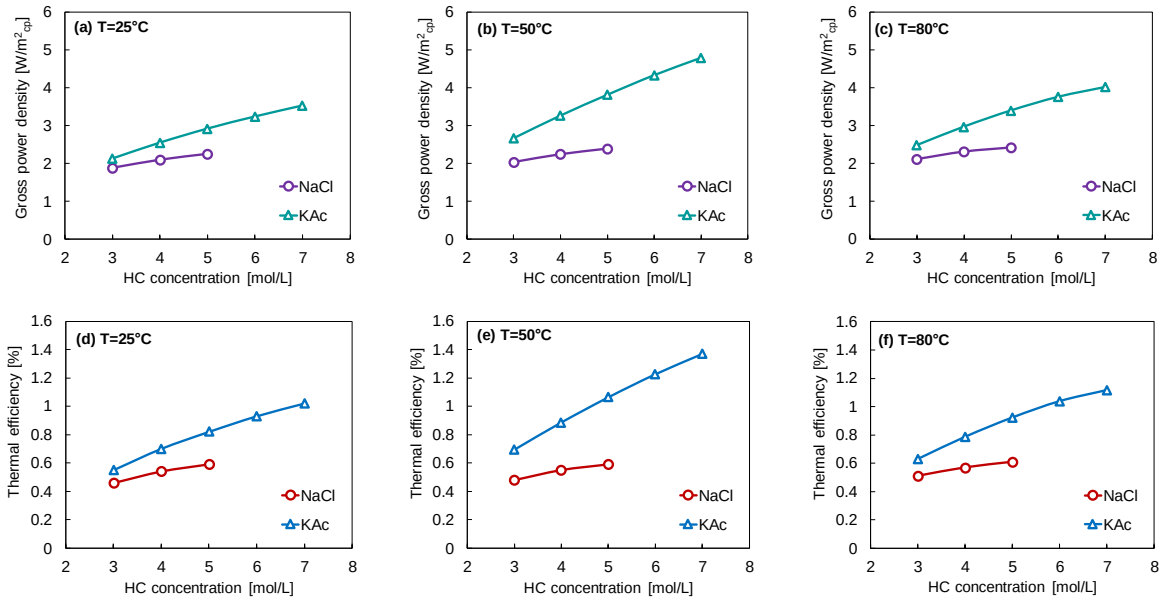

Fig. 7. RED-HE performance parameters as a function of the HC inlet concentration and operating temperature (25, 50 and 80 °C), with 12 MED effects, C_{LC}=0.01 mol/L, v_{HC}=0.25 cm/s, v_{LC}=1 cm/s, using standard reference membranes. (a)-(c) Gross power density, (d)-(f) thermal and exergy efficiencies.

4.2. Influence of the number of MED effects

While the results shown in 4.1 refer to a basic reference case, which leads to relatively low performance parameters, here the influence of the number of MED effects on the performance of the RED-MED HE is investigated, in order to assess the best performing conditions for both NaCl and KAc aqueous solutions. In this analysis also high-performing IEMs are considered, as defined in Table 1. The input solutions concentration and velocity are reported in Table 4.

Fig. 8a indicates how the overall thermal efficiency increases with the number of effects for NaCl salt, with both standard reference (solid line) and high-performing membranes (dashed line). This is due to the increase in the efficiency of the MED, i.e. the decrease in the specific

heat consumption. The maximum thermal efficiency achieved with standard reference membranes is 0.9% (4% exergetic), using 24 MED effects. The effect of the operating temperature is negligible in this case. The same trend is obtained with high-performing membranes, although the maximum feasible number of MED effects (with a mean effective temperature driving force in each effect between 1 – 2 °C) is lower (20). This limiting effect is due to the higher BPE of the solution (Fig. S14 of the Supplementary Information file) within the MED, caused by the increase of the inlet HC concentration when passing from standard to high-performing IEMs (3.8 M vs 5 M, see Table 4). The increment of the efficiency when using high-performing IEMs is large, allowing to reach a value of around 6%. This can be explained by the significant reduction of the irreversibility sources (uncontrolled mixing phenomena [34]) that decrease the driving force of the RED process, although it also increases the energy requirements for regeneration. The effect of the operating temperature on the performance with high-performing IEMs is small: at room temperature, the maximum thermal efficiency obtained is 6.1% with 20 MED effects, while at 80°C is 6.3% (28% exergetic), with the same number of effects.

Fig. 8b shows also an increasing trend of efficiency with the number of effects for KAc, although more pronounced than for NaCl. The maximum thermal efficiency obtained with standard reference membranes is of 1.6%, with 12 MED effects and 80 °C, which is 50% higher than the one obtained with NaCl. The maximum number of feasible MED effects is lower than in the case of NaCl due to the higher BPE (see Supplementary Information). The effect of the operating temperature is more pronounced when using high-performing membranes. While at 25 °C and 15 MED effects the thermal efficiency reaches a value of 6.6%, increasing the solutions temperature up to 80 °C results in the maximum value close to 10%, with 12 MED effects. The main advantage of KAc is the higher thermal efficiency obtained with high-performing membranes and high temperature, in comparison with the ones obtained with NaCl.

Such results are extremely interesting in terms of industrial applications, as they highlight how a very high conversion efficiency can be reached with a reasonably low number of MED effects, well in line with industrial standards for MED technology.

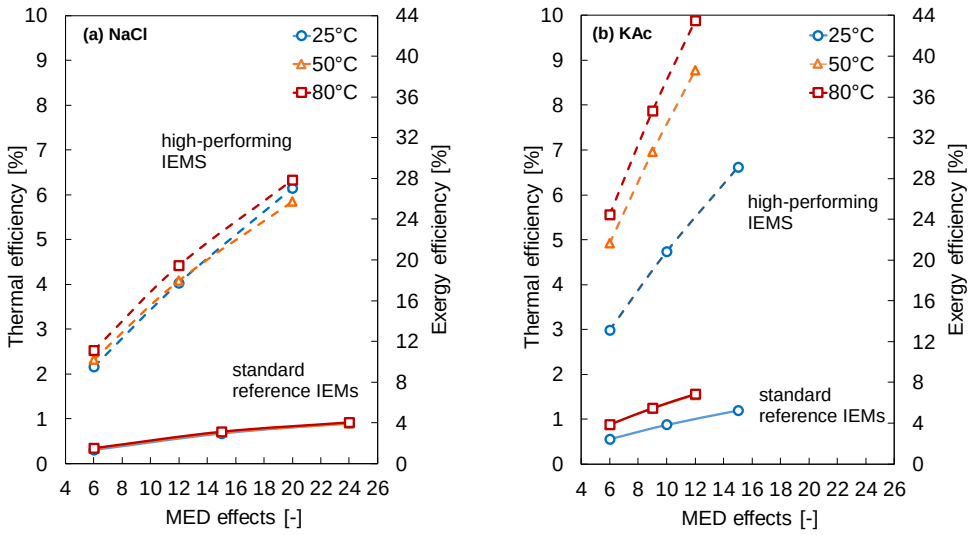

Fig. 8. Thermal and exergy efficiencies for (a) NaCl and (b) KAc salts as a function of the number of MED effects and solutions temperature, using standard reference membranes (solid line) and high-performing membranes (dashed line).

It becomes clear that the potential is extremely high for this technology to reach thermal efficiency values higher than those of other waste heat recovery tecnologies, such as the ORC and thermoelectric generators. A thermal efficiency of almost 10%, as shown in Fig. 8, can be reached by using high-performing membranes, which is a value twice higher than the ORC one for the same heat source temperature.

Looking at the potential for industrial applications, an interesting parameter is the total heat transfer area of the evaporation chambers, normalized to the power generated, which is useful for the estimation of the power production costs of the RED-MED HE. The influence of the number of MED effects on this variable for NaCl is depicted in Fig. 9a. In all cases increases with the number of effects, as expected, due to the reduction in the effective temperature driving force in the evaporators, while the gross power produced does not change. The heat transfer area normalised to the generated power does not change significantly with the operating temperature, reaching a value around 67 m^2/kW with 6 MED effects and standard reference IEMs. Considering high-performing IEMs, this minimum value is decreased to 12.5 m^2/kW (6 MED effects).

It has a similar increasing trend for KAc but with lower values, as depicted in Fig. 9b. At room temperature, an inlet HC solution concentration of 6 M is considered (Table 4), while at 50 and 80 °C this value is increased to 7 M, reducing the maximum feasible number of effects from 15

to 12 and therefore the specific HX area. The minimum value using standard reference membranes is 40 m^2/kW for 6 MED effects and an operating temperature of 80 °C, which is reduced to 7 m^2/kW using high-performing membranes.

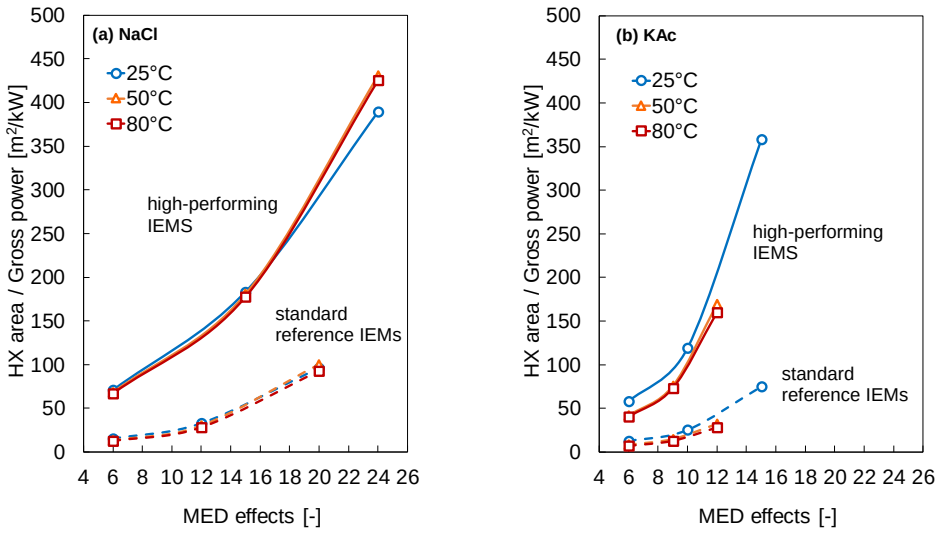

Fig. 9. Specific heat transfer area normalised with the gross power generated for (a) NaCl and (b) KAc salts as a function of the number of MED effects and solutions temperature, using standard reference membranes (solid line) and high-performing membranes (dashed line).

Finally, the effect of the number of effects in the specific thermal consumption for NaCl is presented in Fig. 10a. The higher the number of effects, the lower the sE due to the more effective thermal integration in the MED unit. The influence of the solution temperature is negligible, and also the use of high-performing membranes in the RED unit. A minimum sE of 35 kWh/m^3 is obtained using 24 effects. Fig. 10b reveals also an equivalent decreasing trend with the number of effects for KAc, with both standard reference and high-performing membranes, however, due to the lower maximum feasible number of effects (15) compared to the NaCl case, its minimum value is higher, about 55 kWh/m^3, reached at 25 °C. The influence of the solution temperature is also small in this case, having only a slight difference between 25 °C and 50, 80 °C due to the different HC solution concentration in the concentrate loop (6 M vs 7 M, see Table 4).

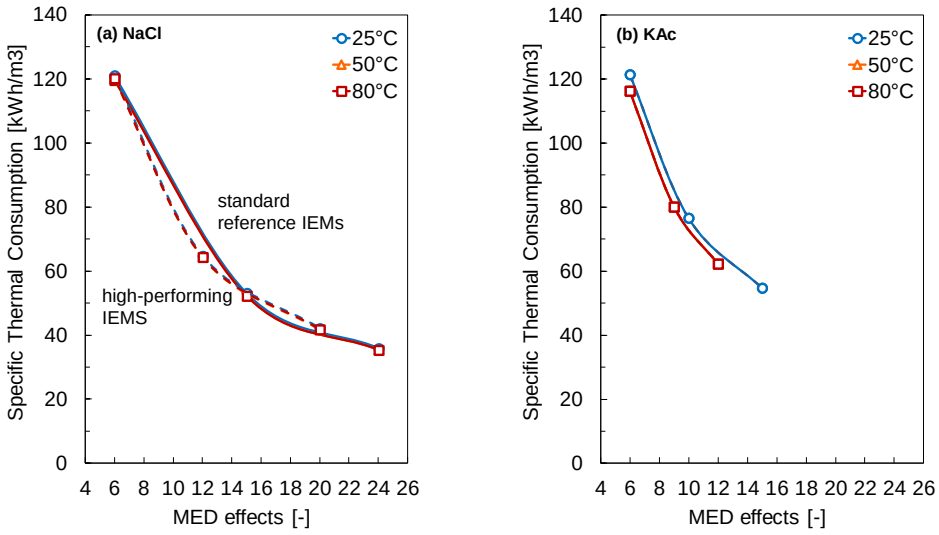

Fig. 10. Specific thermal consumption for (a) NaCl and (b) KAc salts as a function of the number of MED effects and solutions temperature, using standard reference membranes (solid line) and high-performing membranes (dashed line).

5. Conclusions

In this work, the performance of a reverse electrodialysis - multi-effect distillation heat engine is investigated by comparing two different salts, sodium chloride and potassium acetate, and assessing the influenc of reverse electrodialysis operating temperature and the number of multi-effect distillation effects on the process performances. The thermal and exergy efficiency are comparatively evaluated for 25, 50 and 80°C and a variable number of multi-effect distillation effects, using ion exchange membranes with standard reference properties and high-performing properties. Two different schemes of the integrated system are considered: the first one associated with a room temperature operation, and the second one including a thermal integration allowing for reverse electrodialysis operation at a temperature higher than 25 °C, minimizing additional thermal inputs from the waste heat source. The main conclusions of the sensitivity analysis are:

– The use of potassium acetate aqueous solution as the working fluid of the reverse electrodialysis heat engine leads to higher thermal efficiency than considering sodium chloride aqueous solution. Under the investigated conditions, KAc leads to a thermal efficiency of about 10% (43% exergy efficiency), at 80 °C with high-performing membranes and 12 effects. The same system, using NaCl solutions, achieved a thermal efficiency of 6.3% (28% exergy efficiency) at the same temperature, with high-

performing membranes and 20 effects. The better performance of KAc can be mainly attributed to its higher solubility and higher activity coefficient in comparison with NaCl.

- Increasing the reverse electrodialysis operating temperature results in higher overall thermal efficiency, mainly due to the lower electrical resistance and larger power generation in the pile. Although the higher temperature also leads to an increase of the salt and water diffusive fluxes, which are detrimental effects for the performance of the system.
- The use of potassium acetate as working fluid leads to a lower number of effects in the multi-effect distillation unit and therefore lower power-normalised specific heat transfer area, hence reducing the fixed costs associated with the heat exchangers, which represent a major part of the total power production cost in the heat engine.
- The present analysis highlights a very interesting potential of the reverse electrodialysis multi-effect distillation heat engine, which can be a promising technology for waste heat recovery and energy efficiency strategies in the future.

Acknowledgments

This work has been performed within the RED Heat-to-Power project (Conversion of Low Grade Heat to Power through closed loop Reverse Electro-Dialysis) – Horizon 2020 program, Grant Agreement no. 640667.

The authors would like to acknowledge Fujifilm Manufacturing Europe B.V. for their support and for providing information on ion exchange membranes properties.

Nomenclature

Variables

A	Area, m^2
b	Membrane's width, m
C	Concentration, mol/L
d_i	Inner diameter, m
E	Voltage, V
F	Faraday constant, C/mol

H	Height of each effect, m
i, I	Electric current, A
j_f	Friction factor, -
L	Membrane's length, m
m	Molality, mol/kg
$\dot{m}$	Mass flow rate, kg/s
N_{cp}	Number of cell pairs, -
N_p	Number of passes, -
p	Pressure, Pa
P	Power, W
P_s	Salt permeability, m^2/s
P_w	Water permeability, m/(Pa·s)
P_Q	Heat rate, W
Q	Volumetric flow rate, m^3/s
R	Electrical resistance, $\Omega \cdot m^2$
R_g	Gas constant, J/(mol·K)
sA	Specific heat transfer area, $m^2/(kg/s)$
sE	Specific thermal energy, $kWh/m^3_{distillate}$
T	Temperature, K or °C
U	Overall heat transfer coefficient, $W/(m^2 \cdot K)$
v	Velocity, cm/s

Acronyms and abbreviations

AEM	Anion Exchange Membrane
BPE	Boiling Point Elevation
CEM	Cation Exchange Membrane
EES	Engineering Equation Solver
FB	Flash Box
FC	Final Condenser
FF	Forward-Feed
HC	High Concentration
HE	Heat Engine
HT	High Temperature
HX	Heat eXchanger
IEM	Ion Exchange Membrane
LC	Low Concentration

MD	Membrane Distillation
MED	Multi-Effect Distillation
NTU	Number of Transfer Units
PH	Preheater
PHX	Plate Heat Exchanger
PRO	Pressure Retarded Osmosis
RED	Reverse ElectroDialysis
RH	Reheater
RT	Room Temperature
SGP	Salinity Gradient Power

Subscripts

av	Average
c	Condenser
cw	Cooling water
cp	Cell pair
d	Density
D	Distillate
f	Feed
H	Height
HC	High concentration
L	Load
LC	Low concentration
m	Membrane
M1	Mixer 1
p	Pump
preh	Preheater
s	Salt
th	Thermal
w	Water
wh	Waste heat
X	Exergetic

Greek

α	Permselectivity, -
δ	Thickness, m
γ	Activity coefficient, -
η	Efficiency, -
θ	Polarization coefficient, -
λ	Enthalpy of vaporization, J/kg
ϵ	Effectiveness, -
ρ	Density, kg/m^3

References

[1] International Energy Agency. Key world energy statistics. 2017.

[2] Gou X, Xiao H, Yang S. Modeling, experimental study and optimization on low-temperature waste heat thermoelectric generator system. Appl Energy 2010;87:3131–6. doi:10.1016/j.apenergy.2010.02.013.

[3] Kosmadakis G. Estimating the potential of industrial (high-temperature) heat pumps for exploiting waste heat in EU industries. Appl Therm Eng 2019;156:287–98. doi:10.1016/j.applthermaleng.2019.04.082.

[4] Brückner S, Liu S, Miró L, Radspieler M, Cabeza LF, Lävemann E. Industrial waste heat recovery technologies: An economic analysis of heat transformation technologies. Appl Energy 2015;151:157–67. doi:10.1016/j.apenergy.2015.01.147.

[5] Papapetrou M, Kosmadakis G, Cipollina A, La Commare U, Micale G. Industrial waste heat: Estimation of the technically available resource in the EU per industrial sector, temperature level and country. Appl Therm Eng 2018;138:207–16. doi:10.1016/J.APPLTHERMALENG.2018.04.043.

[6] Tamburini A, Cipollina A, Papapetrou M, Piacentino A, Micale G. 7 – Salinity gradient engines. Sustain. Energy from Salin. Gradients, 2016, p. 219–56. doi:10.1016/B978-0-08-100312-1.00007-9.

[7] Maisonneuve J, Laflamme CB, Pillay P. Experimental investigation of pressure retarded osmosis for renewable energy conversion: Towards increased net power. Appl Energy 2016;164:425–35. doi:10.1016/j.apenergy.2015.12.007.

[8] Altaee A, Palenzuela P, Zaragoza G, AlAnezi AA. Single and dual stage closed-loop pressure retarded osmosis for power generation: Feasibility and performance. Appl Energy 2017;191:328–45. doi:10.1016/j.apenergy.2017.01.073.

[9] Maisonneuve J, Pillay P, Laflamme CB. Pressure-retarded osmotic power system model considering non-ideal effects. Renew Energy 2015;75:416–24. doi:10.1016/J.RENENE.2014.10.011.

[10] Tedesco M, Scalici C, Vaccari D, Cipollina A, Tamburini A, Micale G. Performance of

the first reverse electrodialysis pilot plant for power production from saline waters and concentrated brines. J Memb Sci 2016;500:33–45. doi:10.1016/j.memsci.2015.10.057.

[11] Kim D han, Park BH, Kwon K, Li L, Kim D. Modeling of power generation with thermolytic reverse electrodialysis for low-grade waste heat recovery. Appl Energy 2017;189:201–10. doi:10.1016/j.apenergy.2016.10.060.

[12] Olkis C, Santori G, Brandani S. An Adsorption Reverse Electrodialysis system for the generation of electricity from low-grade heat. Appl Energy 2018;231:222–34. doi:10.1016/j.apenergy.2018.09.112.

[13] Tufa RA, Pawlowski S, Veerman J, Bouzek K, Fontananova E, di Profio G, Velizarov S, Goulão Crespo J, Nijmeijer K, Curcio E. Progress and prospects in reverse electrodialysis for salinity gradient energy conversion and storage. Appl Energy 2018;225:290–331. doi:10.1016/j.apenergy.2018.04.111.

[14] Altaee A, Millar GJ, Zaragoza G. Integration and optimization of pressure retarded osmosis with reverse osmosis for power generation and high efficiency desalination. Energy 2016;103:110–8. doi:10.1016/J.ENERGY.2016.02.116.

[15] Touati K, Tadeo F. Green energy generation by pressure retarded osmosis: State of the art and technical advancement—review. Int J Green Energy 2017;14:337–60. doi:10.1080/15435075.2016.1255633.

[16] Conversion of Low Grade Heat to Power through closed loop Reverse ElectroDialysis—Horizon 2020 programme, Project Number: 640667: www.red-heat-to-power.eu n.d. https://cordis.europa.eu/project/rcn/193740_en.html (accessed September 4, 2018).

[17] Tamburini A, Tedesco M, Cipollina A, Micale G, Ciofalo M, Papapetrou M, Van Baak W, Piacentino A. Reverse electrodialysis heat engine for sustainable power production. Appl Energy 2017;206:1334–53. doi:10.1016/J.APENERGY.2017.10.008.

[18] Kwon K, Park BH, Kim DDH, Kim DDH. Parametric study of reverse electrodialysis using ammonium bicarbonate solution for low-grade waste heat recovery. Energy Convers Manag 2015;103:104–10. doi:10.1016/J.ENCONMAN.2015.06.051.

[19] Bevacqua M, Carubia A, Cipollina A, Tamburini A, Tedesco M, Micale G. Performance of a RED system with ammonium hydrogen carbonate solutions. Desalin Water Treat 2016;57:23007–18. doi:10.1080/19443994.2015.1126410.

[20] Bevacqua M, Tamburini A, Papapetrou M, Cipollina A, Micale G, Piacentino A. Reverse electrodialysis with NH4HCO3-water systems for heat-to-power conversion. Energy 2017;137:1293–307. doi:10.1016/J.ENERGY.2017.07.012.

[21] Giacalone F, Vassallo F, Griffin L, Ferrari MC, Micale G, Scargiali F, Tamburini A, Cipollina A. Thermolytic reverse electrodialysis heat engine: model development, integration and performance analysis. Energy Convers Manag 2019;189:1–13. doi:10.1016/j.enconman.2019.03.045.

[22] Long R, Li B, Liu Z, Liu W. Hybrid membrane distillation-reverse electrodialysis electricity generation system to harvest low-grade thermal energy. J Memb Sci 2017;525:107–15. doi:10.1016/j.memsci.2016.10.035.

[23] Micari M, Cipollina A, Giacalone F, Kosmadakis G, Papapetrou M, Zaragoza G, Micale G, Tamburini A. Towards the first proof of the concept of a Reverse ElectroDialysis - Membrane Distillation Heat Engine. Desalination 2019;453:77–88. doi:10.1016/j.desal.2018.11.022.

[24] Shahzad MW, Burhan M, Ang L, Ng KC. Energy-water-environment nexus underpinning future desalination sustainability. Desalination 2017;413:52–64. doi:10.1016/J.DESAL.2017.03.009.

[25] Ruiz-Aguirre A, Andrés-Mañas JA, Fernández-Sevilla JM, Zaragoza G. Experimental characterization and optimization of multi-channel spiral wound air gap membrane distillation modules for seawater desalination. Sep Purif Technol 2018;205:212–22. doi:10.1016/J.SEPPUR.2018.05.044.

[26] Hu J, Xu S, Wu X, Wu D, Jin D, Wang P, Leng Q. Theoretical simulation and evaluation for the performance of the hybrid multi-effect distillation—reverse electrodialysis power generation system. Desalination 2018;443:172–83. doi:10.1016/j.desal.2018.06.001.

[27] Palenzuela P, Micari M, Ortega-Delgado B, Giacalone F, Zaragoza G, Alarcón-Padilla D-C, et al. Performance Analysis of a RED-MED Salinity Gradient Heat Engine. Energies 2018;11:3385. doi:10.3390/en11123385.

[28] Kosmadakis G, Landelle A, Lazova M, Manolakos D, Kaya A, Huisseune H, Karavas CS, Tauveron N, Revellin R, Haberschill P, De Paepe M, Papadakis G. Experimental testing of a low-temperature organic Rankine cycle (ORC) engine coupled with concentrating PV/thermal collectors: Laboratory and field tests. Energy 2016;117:222–36. doi:10.1016/j.energy.2016.10.047.

[29] Champier D. Thermoelectric generators: A review of applications. Energy Convers Manag 2017;140:167–81. doi:10.1016/j.enconman.2017.02.070.

[30] Giacalone F, Olkis C, Santori G, Cipollina A, Brandani S, Micale G. Novel solutions for closed-loop reverse electrodialysis: Thermodynamic characterisation and perspective analysis. Energy 2019;166:674–89. doi:10.1016/j.energy.2018.10.049.

[31] Benneker AM, Rijnaarts T, Lammertink RGH, Wood JA. Effect of temperature gradients in (reverse) electrodialysis in the Ohmic regime. J Memb Sci 2018;548:421–8. doi:10.1016/J.MEMSCI.2017.11.029.

[32] Długołecki P, Gambier A, Nijmeijr K, Wessling M. Practical Potential of Reverse Electrodialysis As Process for Sustainable Energy Generation. Environ Sci Technol 2009;43:6888–94.

[33] Daniilidis A, Vermaas DA, Herber R, Nijmeijer K. Experimentally obtainable energy from mixing river water, seawater or brines with reverse electrodialysis. Renew Energy 2014;64:123–31. doi:10.1016/J.RENENE.2013.11.001.

[34] Giacalone F, Catrini P, Tamburini A, Cipollina A, Piacentino A, Micale G. Exergy analysis of reverse electrodialysis. Energy Convers Manag 2018;164:588–602. doi:10.1016/j.enconman.2018.03.014.

[35] Klein SA. Engineering Equation Solver Software (EES) 2013.

[36] El-Dessouky HTHT, Ettouney HMHM. Chapter 4 - Multiple Effect Evaporation. Amsterdam: Elsevier; 2002. doi:http://0-dx.doi.org.fama.us.es/10.1016/B978-044450810-2/50006-3.

[37] Ortega-Delgado B, García-Rodríguez L, Alarcón-Padilla D-C. Opportunities of improvement of the MED seawater desalination process by pretreatments allowing high-temperature operation. Desalin Water Treat 2017;97. doi:10.5004/dwt.2017.21679.

[38] Çengel YA. Heat transfer : a practical approach . 2nd ed. Boston: McGraw-Hill; 2003.

[39] Incropera FP, DeWitt DP. Fundamentals of heat and mass transfer. 5th ed. New York: John Wiley; 2002.

[40] Bockris JOM, Reddy AKN. Modern Electrochemistry Vol. 1. Ionics. 2nd ed. 1998.

[41] Burakowski A, Gliński J. Hydration of ions containing aliphatic chains. Chem Phys Lett 2009;468:184–7. doi:10.1016/J.CPLETT.2008.12.019.

[42] Pitzer KS. Activity Coefficients in Electrolyte Solutions. Boca Raton: CRC Press; 1991. doi:10.1201/9781351069472.

[43] Micale G, Cipollina A, Rizzuti L. Seawater Desalination: Conventional and Renewable Energy Processes. Seawater Desalin. Conv. Renew. Energy Process., 2009. doi:10.1007/978-3-642-01150-4.